Ab initio structure modeling of complex thin-film oxides: thermodynamical stability of TiC/thin-film alumina

Jochen Rohrer,[1,*] Carlo Ruberto,[1,2] and Per Hyldgaard[1]

[1] *BioNano Systems Laboratory, Department of Microtechnology, MC2, Chalmers University of Technology, SE-412 96 Gothenburg*
[2] *Materials and Surface Theory Group, Department of Applied Physics, Chalmers University of Technology, SE-412 96 Gothenburg*

(Dated: March 6, 2009)

We present an efficient and general method to identify promising candidate configurations for thin-film oxides and to determine structural characteristics of (metastable) thin-film structures using *ab initio* calculations. At the heart of this method is the complexity of the oxide bulk structure, from which a large number of thin films with structural building blocks, that is motifs, from metastable bulk oxide systems can be extracted. These span a coarse but well-defined network of initial configurations for which density functional theory (DFT) calculations predict and implement dramatic atomic relaxations in the corresponding, resulting thin-film candidates. The network of thin-film candidates (for various film thicknesses and stoichiometries) can be ordered according to their variation in *ab initio* total energy or in *ab initio* equilibrium Gibbs free energy. Analysis of the relaxed atomic structures for the most favored structures gives insight into the nature of stable and metastable thin-film oxides. We investigate ultrathin alumina nucleated on TiC as a model system to illustrate this method. The stable α- and metastable κ-Al_2O_3 bulk structures lead to an alumina-film candidate-space that consists of 38 configurations for a given film thickness, including three different stoichiometries. We identify the stoichiometries that are relevant in equilibrium with an O environment from *ab initio* thermodynamics calculations of the relaxed configurations. These relevant stoichiometries are $Al_{4n-4}O_{6n}$ and $Al_{4n-2}O_{6n}$ (only in equilibrium at extremely low O chemical potentials), with $n = 2$, 3, 4 identifying the number of oxygen layers. The films with $Al_{4n}O_{6n}$ stoichiometry are not stable for any allowed value of the O chemical potential. Our analysis of the atomic structure shows that the favorable structural motifs of the relaxed films heavily differ from those in the bulk. In particular the number of tetrahedrally coordinated Al ions is much higher in the films and the corresponding tetrahedra are oriented differently than in the bulk. This finding of additional or novel favorable motifs documents that the method is capable of catching thin-film candidates with a structural nature that is not explicitly included in the network of initial thin-film configurations. Our analysis also shows that the thermodynamically most stable TiC/$Al_{4n-4}O_{6n}$ systems decay into a partly decoupled TiC/O/$Al_{4n-4}O_{6n-6}$ system, with only a weak binding of the $Al_{4n-4}O_{6n-6}$ film on the TiC/O substrate.

PACS numbers: 68.55.-a, 68.47.Gh, 68.35.-p, 64.75.St

I. INTRODUCTION

Understanding the atomic and electronic structure of thin-film oxides is of significant industrial and fundamental importance and a huge challenge at the same time. Bulk oxides are characterized by a strong ionicity, which often results into a tendency for a high structural flexibility and an organization in a large number of different stable and metastable phases. Prominent examples can be found among aluminum oxides,[1] titanium oxides,[2] vanadium oxides,[3] or hafnium oxides.[4] For an ultra-thin film, the structural variety of the oxide can be even larger.[5,6] The mainly insulating character of oxides makes accurate experimental atomic and electronic structure determinations difficult, since high-resolution techniques (low energy electron diffraction (LEED),[5] scanning tunneling microscopy (STM),[6] transmission electron microscopy (TEM),[7] scanning electron microscopy(SEM),[8] ...) mainly use charged particles. Theory assisted methods, such as density functional theory (DFT) calculations, are of high complementary value. However, when modeling thin films that are adsorbed on a substrate, relatively large surface unit cells are often needed. As a consequence, an enormous number of possible atomic configurations for the film arises, and a structure determination by straightforward energy calculations of all possible candidates becomes computationally intractable.

The nucleation of alumina on TiC provides an illustration of the complexity and importance of predicting and understanding atomic structure in oxides, ultra-thin oxide films and their interfaces. Multilayers of TiC/alumina are highly relevant for industrial application as wear-resistant coatings on cemented-carbide cutting tools.[9] They are commonly fabricated by chemical vapor deposition (CVD). Typically, the α-Al_2O_3 (stable in the bulk) and κ-Al_2O_3 (metastable in the bulk) phases are obtained with relative orientations are $\alpha(0001)||$TiC(111) and $\kappa\{001\}||$TiC(111).[10] However, these ordered structures only arise when the alumina possesses a considerable thickness. The nucleation of alumina on TiC involves the formation of ultra-thin alumina films. Insight into the detailed, atomic configuration in the

ultra-thin films is essential because their structure may strongly influence the subsequent growth.[11] A complete search through all possible atomic thin-film configurations by total energy calculations is, however, extremely difficult.[12]

Of course, *ab initio* molecular dynamics (MD)[13] is a powerful tool that can generally sample typical, and hence relevant, structural configurations (for a given film thickness and stoichiometry) by simply following the atomic dynamics at some elevated temperature. The use of density functional theory (DFT) to evaluate the forces on the constituent atoms makes this a highly accurate, but also costly, method. For strongly ionic materials like (thin-film) alumina drastic charge rearrangements occur with the motion of every single atom. As this calls for very small time steps, formidable *ab initio* MD simulation times can be expected. Moreover, for a study of thin-film nucleation it is imperative to explore possible candidate structures for a range of different thicknesses and stoichiometric compositions. It is clear that some alternative, accelerated search method is desirable.

In this paper, we suggest an *ab initio* method to search for the structural elements of thermodynamically stable and metastable thin-film oxide configurations nucleated on metallic substrates. The *ab initio* method avoids costly molecular-dynamics simulations but invokes atomic relaxations specified by underlying DFT calculations of the atomic forces. The approach makes use of the complexity of oxide bulk structures and their ionicity. The method is illustrated for the TiC/thin-film alumina system that we investigate as an example. We start with a coarse sampling of the thin-film configuration space by relaxing all possible films that consist of partial alumina bulk structures. Due to their stability in the bulk they can be assumed as promising initial configurations that contain structural elements, that is motifs, relevant for the actual stable and metastable thin-film structures. To further trigger relaxations towards other configurations that do not possess a partial bulk structure, we slightly distort the unrelaxed candidates. The relaxed atomic structures that are energetically favorable and that differ essentially from the partial bulk structures can be used to design new candidates with a similar structure. The procedure could then be iterated until self-consistency is reached. For thin-film configurations that differ in their stoichiometry, the energy criterion is replaced by the criterion of lowest Gibbs free energy. The latter we calculate from *ab initio* thermodynamics.[14,15,16]

The paper is organized as follows: Section II summarizes the properties of alumina and TiC that are relevant for TiC/thin-film alumina. In Sec. III we derive all TiC/thin-film alumina initial configurations that are consistent with the bulk structure of the respective materials. The details concerned with the computation of total and Gibbs free energies are discussed in Sec. IV. In Sec. V, we present our results on the energetics and thermodynamical stability of thin-film alumina. An analysis of the atomic structure of relaxed films is given in Sec. VI.

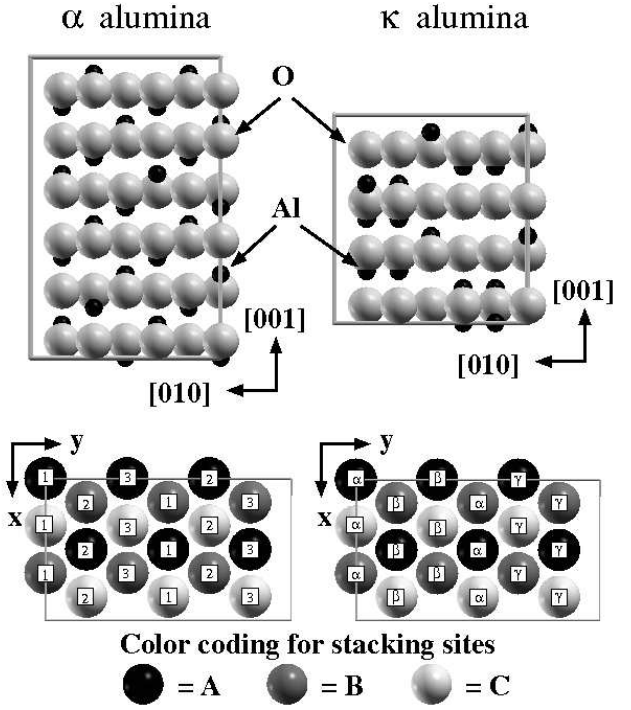

FIG. 1: Bulk structures of α- (left) and κ-Al_2O_3 (right) within orthorhombic unit cells. The top panels show side views along [100]. The bottom panels define the atomic site labeling within each (001) atomic layer.

Reflection about	Effect on					
	$A(a)$	$B(b)$	$C(c)$	$\alpha(1)$	$\beta(2)$	$\gamma(3)$
xz-plane	$A(a)$	$B(b)$	$C(c)$	$\alpha(1)$	$\gamma(3)$	$\beta(2)$
yz-plane	$A(a)$	$C(c)$	$B(b)$	$\alpha(1)$	$\beta(2)$	$\gamma(3)$

TABLE I: Mapping of stacking and site labels (as defined in Fig. 1) under mirror transformations. A reflection about the xz-plane leads for example to a relabeling of $c_\beta \rightarrow c_\gamma$.

In Sec. VII, we discuss our results and Sec. VIII, contains our conclusions.

II. MATERIALS BACKGROUND

We first summarize the bulk and surface properties of alumina and TiC that are relevant for our thin-film modeling method.

A. Stable and metastable Al_2O_3 bulk structures

Figure 1 shows a schematics of the bulk structures of α (trigonal unit cell, space group $R\bar{3}c$) and κ alumina (orthorhombic unit cell, space group $Pna2_1$).[17,18] Along the $\alpha[0001]$ and $\kappa[001]$ directions, both alumina phases are composed of alternating O and Al layers, the latter

splitting up into two sublayers. In α-Al_2O_3, all Al ions are octahedrally (O) coordinated. In κ-Al_2O_3, the coordination alternates. In every second layer all Al ions have octahedral coordination. In the other layers 50 % of the Al ions is octahedrally and 50 % tetrahedrally (T) coordinated. All tetrahedra point in the [001] direction.

To facilitate a parallel treatment of α- and κ-Al_2O_3, we choose an orthorhombic unit cell for the representation of both alumina phases, so that $\alpha[0001]_{\rm hex} \Leftrightarrow \alpha[001]_{\rm ortho}$. The associated calculated lattice parameters are a = 4.798 (4.875) Å, b = 8.311 (8.378) Å, and c = 13.149 (9.018) Å for α (κ),[18,19] which is in good agreement with experimental data.[20,21]

The atomic structures of α- and κ-Al_2O_3 can be described as follows. We denote the stacking sites of full O layers by capital letters. For the Al layers small letters with subscript (Arabic numerals for α, Greek letters for κ) are used. The subscript relates each two Al sites per unit cell, see Fig. 1 for a detailed definition of each label. For κ this notation is identical to the one introduced in Ref. 18, whereas for α it is a slightly modified version of the one of Ref. 22, where Greek superscripts are used for the labeling of Al vacancies. With this notation, the bulk stackings are[18,22]

$$\begin{aligned} \alpha[0001]: &\quad Ac_3c_2Bc_1c_3Ac_2c_1Bc_3c_2Ac_1c_3Bc_2c_1 \\ \kappa[001]: &\quad Ab_\gamma c_\beta Bc_\alpha c_\gamma Ac_\beta b_\gamma Cb_\alpha b_\beta\ . \end{aligned} \tag{1}$$

Reflections about the xz-plane [$\Leftrightarrow$ (010)] or yz-plane [$\Leftrightarrow$ (100)] are symmetries of the bulk. Although the structure is not invariant under these transformations, the transformed structures are equivalent to the non-transformed one. The effects of the mirror transformations on individual stacking sites are listed in Table I. Reflection about the xz-plane corresponds to interchanging $\beta \leftrightarrow \gamma$ and $2 \leftrightarrow 3$, reflection about the yz-plane to $C \leftrightarrow B$ and $c \leftrightarrow b$.

B. TiC(111) surface and reactivity

Bulk TiC possesses NaCl structure with a theoretical lattice parameter[23] $a = 4.332$ Å (in good agreement with the experimental value[24] $a_{\rm exp} = 4.33$ Å). Along the [111] direction, it is thus composed of close-packed alternating Ti and C layers. The stacking sequence of one repeat unit is $ABCABC$.

We only consider Ti-terminated TiC(111) surfaces. This choice is motivated by the stronger binding of Ti to the C-terminated surface compared to the binding of C to the Ti-terminated surface.[23] Furthermore, there is experimental evidence for a preferred Ti termination upon annealing.[25]

On Ti-terminated TiC(111), atomic O adsorbs much more strongly than atomic Al (about three times as strong).[23] We therefore identify the first alumina layer above the TiC/Al_2O_3 interface plane as an O layer. According to Refs. 23 and 26, both single O atoms and a full O monolayer prefer adsorption in the fcc site. By defining the TiC stacking such that the fcc site on its (111) surface is labeled by an A stacking letter, the hcp site by B, and the top site by C, the position of the first O layer is therefore fixed to A stacking. For the monolayer, our calculated Ti–O layer separation along TiC[111] is $d_{\rm Ti\text{-}O} = 0.89$ Å.

III. THIN-FILM IDENTIFICATION METHOD

We seek a characterization of alumina nucleation on TiC and identify promising thin-film alumina structure-candidates for different oxide layer thicknesses and stoichiometries. This section describes in detail the proposed method for finding promising initial configurations for TiC/thin-film alumina candidates. First, we derive all the TiC/alumina interface configurations that are consistent with the respective bulk structures and that take into account the adsorption properties of TiC(111). Then, we obtain all the initial thin-film configurations that consist of partial bulk alumina by truncating these interface sequences.

A. TiC/alumina interface structures

Table II lists all the TiC/α-Al_2O_3 and TiC/κ-Al_2O_3 interfaces that are conform with the respective bulk structures and that start with an O layer in fcc (A) site on the Ti-terminated TiC (111) surface. These stacking sequences are found as follows:

We observe that any of the O layers in the listing (1) can be chosen as the initial alumina layer. This layer must be translated to an A site, which can be achieved by cyclic permutations. For the C sites to be translated to A sites we need one cyclic permutation, for B sites to be translated to A sites we need two. All other sites are relabeled accordingly. For example, for $C \rightarrow A$, we have $A \rightarrow B$ and $B \rightarrow C$. For the Al positions the corresponding relabeling has to be performed, keeping the subscripts [α (1), ...] fixed.

Next, we note that the fixed stacking sequence of the TiC substrate breaks the symmetry associated with a reflection about the yz-plane. Hence, for each alumina sequence, we need to consider an additional one, which is obtained by interchanging $B(b) \leftrightarrow C(c)$.

Finally, we exploit that reflection about the xz-plane is still a symmetry of TiC/alumina since the TiC is composed of fully occupied layers. Hence, alumina sequences that are related by $\beta \leftrightarrow \gamma$ ($2 \leftrightarrow 3$) are equivalent.

For α-Al_2O_3, all O layers are equivalent. Therefore it is sufficient to focus on the first O layer, which is already in A stacking. Also, $\alpha[001] \Leftrightarrow \alpha[00\bar{1}]$ and thus only the symmetry breaking associated with the reflection about the yz-plane needs to be considered. As a result, only two possible interfacial configurations have to be taken into account (see Table II, left column).

TiC/α[0001]	TiC/κ[001]	TiC/κ[00$\bar{1}$]
TiC/$Ac_3c_2Bc_1c_3Ac_2c_1Bc_3c_2Ac_1c_3Bc_2c_1$	TiC/$Ab_\gamma c_\beta Bc_\alpha c_\gamma Ac_\beta b_\gamma Cb_\alpha b_\beta$	TiC/$Ab_\beta b_\alpha Cb_\gamma c_\beta Ac_\gamma c_\alpha Bc_\beta b_\gamma$
TiC/$Ab_2b_3Cb_1b_2Ab_3b_1Cb_2b_3Ab_1b_2Cb_3b_1$	TiC/$Ab_\alpha b_\gamma Cb_\beta a_\gamma Ba_\alpha a_\beta Ca_\gamma b_\beta$	TiC/$Ab_\beta a_\gamma Ca_\beta a_\alpha Ba_\gamma b_\beta Cb_\gamma b_\alpha$
	TiC/$Ac_\beta b_\gamma Cb_\alpha b_\beta Ab_\gamma c_\beta Bc_\alpha c_\gamma$	TiC/$Ac_\gamma c_\alpha Bc_\beta b_\gamma Ab_\beta b_\alpha Cb_\gamma c_\beta$
	TiC/$Ac_\alpha c_\beta Bc_\gamma a_\beta Ca_\alpha a_\gamma Ba_\beta c_\gamma$	TiC/$Ac_\gamma a_\beta Ba_\gamma a_\alpha Ca_\beta c_\gamma Bc_\beta c_\alpha$

TABLE II: TiC(111)/alumina interface configurations that respect the bulk structure of α- and κ-Al_2O_3 and start with an O layer in fcc site on the Ti-terminated TiC(111). The TiC stacking of the surface region is defined as $\ldots ABCABC$.

For κ-Al_2O_3, only every second O layer is equivalent and $\kappa[001]$ is not equivalent to $\kappa[00\bar{1}]$. Therefore, we need to consider both directions, any two consecutive bulk O layers, and the effect of the symmetry breaking. This results in four different configurations for each direction (see Table II, middle and right columns).

B. TiC/thin-film alumina candidate structures

We obtain the network of initial thin-film alumina configurations in three steps. In the first step, we truncate the TiC/alumina interface sequences in Table II after a full Al layer. The number of O layers n defines the thickness of the film. In a second step, the resulting configurations are distorted by placing the Al sublayers into one and the same plane, exactly in between the two neighboring O layers. In the third step, we vary the stoichiometry by removing Al ions from the surface in accordance with the bulk space group, *i.e.*, only Al pairs that belong to the same stacking label are removed.

In this way, for each thickness we generate three stoichiometry classes: $Al_{4n}O_{6n}$, $Al_{4n-2}O_{6n}$, and $Al_{4n-4}O_{6n}$, corresponding to the removal of zero, one, and two Al pairs, respectively.

For the α-$Al_{4n-2}O_{6n}$ films, we only consider the surface Al pair that has no direct neighbor in the layer below. With this choice, we minimize the electrostatic energy. We have confirmed the quality of this choice by comparing the total energy for some configurations with different choices of the surface Al pair.

For the κ-$Al_{4n-2}O_{6n}$ films, there is no such simple argument and we choose to allow for both possible Al pairs. As a result, the number of κ-$Al_{4n-2}O_{6n}$ configurations is twice as large as the number of κ-$Al_{4n-4}O_{6n}$ or κ-$Al_{4n}O_{6n}$ configurations.

In Tables III–V, all candidates found by the described procedure are listed for films with thicknesses $n = 2$, 3, and 4 (for thermodynamical reasons, see Sec. V B, no $Al_{16}O_{24}$ configurations are considered).

IV. *AB INITIO* METHOD

A. Total energies and atomic relaxations

All calculations are performed with the DFT plane-wave code dacapo[27] using ultra-soft pseudopotentials[28] and the PW91 exchange-correlation[29] functional.

We use a supercell approach and model the TiC/thin-film alumina by slab geometry. The basal plane dimensions of the supercell are chosen to fit the 3×2 TiC(111) surface (5.306×9.190 Å^2) and the height is fixed to 30 Å, ensuring a vacuum thickness of at least 13 Å.

The TiC is modeled by four atomic bilayers (with six Ti and six C atoms per bilayer). The alumina films contain six O atoms per O layer and a varying number of Al atoms, depending on the film stoichiometry. In total, the slabs contain between 64 (Al_4O_{12} films) and 86 atoms ($Al_{14}O_{24}$ films).

We use a 400 eV plane-wave cutoff and a 4×2×1 Monkhorst-Pack[30] k-point sampling. Electrostatic effects arising from the charge asymmetry in the slab are corrected for by a dipole correction. The atomic relaxations are performed until all interatomic forces are smaller than 0.05 eV/Å. This choice has proven a good accuracy at acceptable CPU times for α- and κ-Al_2O_3 surfaces[19] and for TiC/alumina interface calculations.[31] The presented DFT calculations amount to a total of one million CPU hours on modern supercomputing facilities.

B. Equilibrium Thermodynamics

At non-zero temperature T and pressure p the stability of any system is governed by the Gibbs free energy G.

Surfaces. Figure 2(a) shows a typical atomic setup used for calculating surface energies using slab geometry.[32] For alumina, the average surface Gibbs free energy $\sigma_{\rm av}$ of the pair of alumina surfaces represented by the slab is defined by

$$\sigma_{\rm av} = \frac{1}{2}\left(\sigma^+ + \sigma^-\right) = \frac{1}{2A}\left(G_{\rm slab} - n_{\rm Al}\mu_{\rm Al} - n_{\rm O}\mu_{\rm O}\right) \ . \quad (2)$$

Here σ^+ and σ^- correspond to the two surface energies associated with each side of the slab ($\sigma_{\rm av} = \sigma^+ = \sigma^- = \sigma$ for a symmetric slab), $G_{\rm slab}$ is the Gibbs free energy of the slab that contains $n_{\rm Al}$ Al and $n_{\rm O}$ O atoms, and $\mu_{\rm Al}$ and $\mu_{\rm O}$ are the chemical potentials of Al and O respectively.

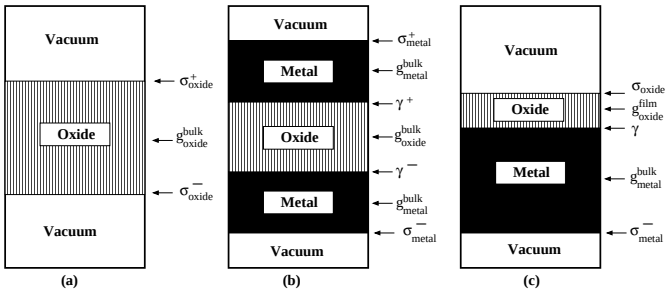

FIG. 2: Schematics of atomic setup for calculations of (a) (oxide) surfaces (b) (metal/oxide) interfaces and (c) thin-film oxide on a metal substrate. The arrows point to the regions in the slabs where the bulk ($g^{\rm bulk}$), surface (σ), interface (γ) or thin-film ($g^{\rm film}$) contributions to the Gibbs free energy are located. We emphasize that, in general $g^{\rm bulk}_{\rm oxide} \neq g^{\rm film}_{\rm oxide}$.

In equilibrium with an O environment, the stoichiometrically weighted sum of the Al and O chemical potentials must equal the Gibbs free energy per stoichiometric unit of alumina $g_{\rm Al_2O_3}$,

$$2\mu_{\rm Al} + 3\mu_{\rm O} = g_{\rm Al_2O_3} \ , \qquad (3)$$

so that $\sigma_{\rm av}$ can be rewritten as a function of the O chemical potential only.

Interfaces. Figure 2(b) shows a schematics of of a typical slab geometry used to calculate interface energies.[33] For metal/alumina interfaces, the stability is determined by the interface Gibbs free energy γ. Using the slab geometry of Fig. 2(b), the average interface energy is calculated as

$$\begin{aligned}\gamma_{\rm av} &= \frac{1}{2}\left(\gamma^+ + \gamma^-\right) \\ &= \frac{1}{2A}\left(G_{\rm slab} - \sum_i n_i\mu_i - A\sigma^+_{\rm metal} - A\sigma^-_{\rm metal}\right) \\ &= \frac{1}{2A}\Bigg(G_{\rm slab} - n_{\rm metal}g_{\rm metal} - \frac{n_{\rm Al}}{2}g_{\rm Al_2O_3} - \\ &\quad \left(n_{\rm O} - \frac{3n_{\rm Al}}{2}\right)\mu_{\rm O} - A\sigma^+_{\rm metal} - A\sigma^-_{\rm metal}\Bigg) \ . \qquad (4)\end{aligned}$$

Here γ^+ and γ^- are the interface energies corresponding to the two interfaces in Fig. 2(a), $G_{\rm slab}$ is the Gibbs free energy of the total slab, and n_i and μ_i are the number and chemical potentials of the different atomic species ($i \in$ {Al, O, or metal}). In the last equality, we have assumed equilibrium with an O environment and used Eq. 3 to express $\gamma_{\rm av}$ as a function of the O chemical potential only. For a symmetric slab, we have $\gamma_{\rm av} = \gamma^+ = \gamma^- = \gamma$.

TiC/thin-film alumina. Figure 2(c) sketches the atomic setup used for the present thin-film calculations. The stability of TiC/thin-film alumina is governed by three contributions: (i) the surface stability of the thin film (σ), (ii) the stability of the interfacial configuration (γ), and (iii) the internal stability of the thin film itself ($g^{\rm film}_{\rm Al_2O_3}$).

The first two contributions can be expressed by

$$\begin{aligned}A(\gamma+\sigma) &= G_{\rm slab} - n_{\rm TiC}g_{\rm TiC} - n_{\rm Al}\mu_{\rm Al} - n_{\rm O}\mu_{\rm O} - \\ &\quad A\sigma^-_{\rm TiC} \ . \qquad (5)\end{aligned}$$

Because we always consider the same TiC slab (always having identical surface energies) it is convenient to express $n_{\rm TiC}g_{\rm TiC}$ through the calculated Gibbs free energy of a TiC slab

$$G_{\rm TiC} = n_{\rm TiC}g_{\rm TiC} + A\sigma^+_{\rm TiC} + A\sigma^-_{\rm TiC} \ . \qquad (6)$$

The stability of the thin-film system is therefore conveniently described by the Gibbs free energy difference

$$\begin{aligned}\Gamma &= A(\gamma + \sigma - \sigma^-_{\rm TiC} - 2\sigma^+_{\rm TiC}) = \\ &= G_{\rm TiC/alumina} - G_{\rm TiC} - n_{\rm Al}\mu_{\rm Al} - n_{\rm O}\mu_{\rm O} \qquad (7)\end{aligned}$$

Note that for practical reasons we do not normalize Γ by the area of the basal plane of the unit cell, since our unit cells all have the same basal plane.

For the third contribution that governs the stability of thin films, $g^{\rm film}_{\rm Al_2O_3}$, we note that in general the Gibbs free energy per stoichiometric unit may and is expected to differ from that in the bulk, that is, $g^{\rm film}_{\rm Al_2O_3} \neq g_{\rm Al_2O_3}$. We therefore introduce a parameter δ, which measures the difference between the Gibbs free energy of one stoichiometric unit of alumina in a bulk environment and in the film and rewrite the equilibrium condition as

$$2\mu_{\rm Al} + 3\mu_{\rm O} = g_{\rm Al_2O_3} + \delta \ . \qquad (8)$$

The stability-determining quantity for TiC/thin-film alumina configurations can be reformulated from Eqs. 7 and 8:

$$\begin{aligned}\Gamma &= G_{\rm TiC/Al_nO_m} - G_{\rm TiC} - \frac{n_{\rm Al}}{2}\left(g_{\rm Al_2O_3} + \delta\right) \\ &\quad -\left(n_{\rm O} - \frac{3}{2}\ n_{\rm Al}\right)\mu_{\rm O} \ . \qquad (9)\end{aligned}$$

The limits of the physically allowed range of the chemical potentials are defined by Al condensation into fcc Al and O condensation into O_2, *i.e.* $\mu_{\rm Al} < g_{\rm fcc\text{-}Al}$ and $\mu_{\rm O} < \frac{1}{2}\mu_{\rm O_2}$, where $g_{\rm fcc\text{-}Al}$ and $\mu_{\rm O_2}$ are the Gibbs free energy per stoichiometric unit of fcc Al and the chemical potential of O_2, respectively. Combining both inequalities and Eq. 8 yields

$$\frac{1}{3}(g_{\rm Al_2O_3} + \delta - 2g_{\rm fcc\text{-}Al}) < \mu_{\rm O} < \frac{1}{2}\mu_{\rm O_2}. \qquad (10)$$

Although an exact value of δ cannot be calculated, we can estimate δ by calculating energy differences between films that differ by an integer number of stoichiometric units,

$$\delta_{nm} = (E_{\rm Al_nO_m} - E_{\rm Al_{n-4}O_{m-6}} - 2\epsilon_{\rm Al_2O_3})/2 \ , \qquad (11)$$

We find that δ_{nm} is 0.4 eV and 0.7 eV when comparing three and two and four and three layer thick films

for $Al_{4n-4}O_{6n}$ stoichiometry. For $Al_{4n-2}O_{6n}$ stoichiometry the corresponding values are 0.3 eV and 1.2 eV. For $Al_{4n}O_{6n}$ stoichiometry we have only considered three and two layer thick films for which we find $\delta_{nm} = 1.1$ eV.

The fact that the largest values of δ_{nm} are found when calculating the energy differences for the thickest considered films is counterintuitive. We would expect that the difference in Gibbs free energy per stoichiometric units converges towards that of the bulk once the film is thick enough. This shows the difficulties in determining the Gibbs free energy of a thin film properly. The higher values for thicker films may be due to completely different surfaces of the respective films and thus due to surface energies.

In the following, we disregard the fact of a non-zero value and the stoichiometry and thickness dependence of δ, that is, we put $\delta \equiv 0$. We have checked that the resulting uncertainty in Γ, although certainly not negligible, does not change our qualitative results as long as the temperatures are not too high (below 1300 K).

C. *Ab initio* Equilibrium Thermodynamics

For the calculation of the Gibbs free energies and chemical potentials involved in Eq. 9 we use the method described in Ref. 16. Here, we only summarize their arguments and give the computational prescription.

The Gibbs free energy of solid material, that is of the *bulk* or a slab, is essentially independent of the pressure. The temperature dependence is considerably stronger and larger in absolute value. Based on the calculated vibrational surface Gibbs free energy for RuO_2,[16] we estimate the vibrational Gibbs free energy per cell for alumina at $T = 1000$ K to $\Gamma^{\rm vib} \sim 1-2$ eV. Compared to the uncertainty in Γ due the uncertainty in δ, the vibrational contributions can therefore savely be neglected.[34]

We consequently choose to approximate Γ by

$$\Gamma \equiv E_{\rm TiC/Al_nO_m} - E_{\rm TiC} - \frac{n_{\rm Al}}{2}\epsilon_{\rm Al_2O_3} - (n_{\rm O} - \frac{3}{2}\, n_{\rm Al})\, \mu_{\rm O}\ , \quad (12)$$

where $E_{\rm TiC/Al_nO_m}$, $E_{\rm TiC}$, and $\epsilon_{\rm Al_2O_3}$ are DFT total energies of a TiC/Al_nO_m slab, an isolated (clean) TiC slab and one stoichiometric unit of bulk alumina respectively.

To estimate the partial O_2 pressure and the temperature that correspond to different values of $\mu_{\rm O}$, we adopt the ideal gas approximation. This approximation allows us to rewrite $\mu_{\rm O}$ as

$$\mu_{\rm O}(T,p) = \frac{1}{2}\left[\epsilon^{\rm DFT}_{\rm O_2} + \delta\mu_{\rm O_2}(T,p_0) + k_{\rm B}T\ln\frac{p}{p_0}\right]. \quad (13)$$

Here $\epsilon^{\rm DFT}_{\rm O_2}$ is the DFT total energy of the O_2 molecule and $\delta\mu(T,p_0)$ is related to the entropy S and enthalpy H at a fixed pressure p_0, see Ref. 16 for details. To calculate $\delta\mu(T,p_0)$, we use the values of S and H for different temperatures at standard pressure $p_0 = 1$ atm that are tabulated in Ref. 35.

V. RESULTS I: ENERGETICAL AND THERMODYNAMICAL STABILITY

In Tables III–V we list all two, three, and four O layers-thick (initial) alumina-film configurations that are consistent with the bulk α- or κ-Al_2O_3 structure. The configurations are grouped according to their stoichiometry, film thickness, and the phase and orientation of the alumina bulk structures from which they are derived.

For each configuration, we list the stacking sequence and the coordination of the Al ions of the alumina film before relaxation, together with the calculated total energies after relaxation. These energies ($E_{\rm rel}$) are given relative to the energy E_0 of the energetically lowest lying configuration of the same thickness and stoichiometry class, $E_{\rm rel} = E - E_0$.

A. Energetics and metastability

For each thickness and stoichiometry class we use the total energy of the energetically most-favorable configuration (the candidate for the stable thin film structure) to define a zero-point of relative energy differences, $E_{\rm rel} = 0$. We stress, however, that bulk alumina also exists in a number of metastable phases. We may therefore also expect metastable configurations among the thin films.

In our calculation for bulk alumina, we find that the DFT energy difference between the κ and α phases is $\Delta_{\alpha\kappa} \sim 0.7$ eV/Al_2O_3. We use this quantity as an indicative measure of the metastability of the alumina films and define $E_{\rm meta} = 2L_{\rm O}\Delta_{\alpha\kappa}$, where $L_{\rm O}$ is the number of O layers in the alumina film. For stoichiometric films, $2L_{\rm O}$ is equal to the number of stoichiometric Al_2O_3 units in the film. For non-stoichiometric films, it will give an approximate measure of the number of stoichiometric units. We then consider configurations with $E_{\rm rel} \gtrsim E_{\rm meta}$ as unstable and configurations with $0 \le E_{\rm rel} \lesssim E_{\rm meta}$ as potentially metastable. Whether or not they are truly metastable cannot, however, be inferred from our calculations. Such an analysis would require a calculation of the nature of vibrational excitations and is much beyond the present investigation.

For the two, three, and four O layers thick films the criterion is $E_{\rm meta} = 0.28$ eV, 0.42 eV, and 0.56 eV, respectively. In Tables III–V, the configurations that are stable or potentially metastable are underlined. For the $Al_{4n-4}O_{6n}$ stoichiometry class, there are at most two potentially metastable configurations for each alumina film thickness. For $Al_{4n}O_{6n}$, no potentially metastable configurations are found. Among the $Al_{4n-2}O_{6n}$ configurations, metastable films are more common. However, their number decreases as the film thickness increases.

alumina group	Al_4O_{12} films: alumina stacking	coord. of Al ions	E_{rel} (eV/cell)	Al_8O_{18} films: alumina stacking	coord. of Al ions	E_{rel} (eV/cell)	$Al_{12}O_{24}$ films: alumina stacking	coord. of Al ions	E_{rel} (eV/cell)
α	Ac_3c_2B	OO	0.71	$Ac_3c_2Bc_1c_3A$	$OO:OO$	5.02	$Ac_3c_2Bc_1c_3Ac_2c_1B$	$OO:OO:OO$	2.34
α	Ab_2b_3C	OO	0.72	$Ab_2b_3Cb_1b_2A$	$OO:OO$	2.78	$Ab_2b_1Cb_1b_2Ab_3b_1C$	$OO:OO:OO$	2.19
$\kappa[001]$	$Ab_\gamma c_\beta B$	$T_\uparrow O$	8.02	$Ab_\gamma c_\beta Bc_\alpha c_\gamma A$	$T_\uparrow O:OO$	9.03	$Ab_\gamma c_\beta Bc_\alpha c_\gamma Ac_\beta b_\gamma C$	$T_\uparrow O:OO:T_\uparrow O$	7.15
$\kappa[001]$	$\underline{Ab_\gamma c_\beta C}$	$T_\uparrow O$	$\underline{0.01}$	$Ac_\beta b_\gamma Cb_\alpha b_\beta A$	$T_\uparrow O:OO$	2.46	$Ac_\beta b_\gamma Cb_\alpha b_\beta Ab_\gamma c_\beta B$	$T_\uparrow O:OO:T_\uparrow O$	7.26
$\kappa[001]$	$Ac_\alpha c_\beta B$	OO	4.43	$Ac_\alpha c_\beta Bc_\gamma a_\beta C$	$OO:T_\uparrow O$	2.03	$Ac_\alpha c_\beta Bc_\gamma a_\beta Ca_\alpha a_\gamma B$	$OO:T_\uparrow O:OO$	4.05
$\kappa[001]$	$Ab_\alpha b_\gamma C$	OO	2.43	$Ab_\alpha b_\gamma Cb_\beta a_\gamma B$	$OO:T_\uparrow O$	1.39	$Ab_\alpha b_\gamma Cb_\beta a_\gamma Ba_\alpha a_\beta C$	$OO:T_\uparrow O:OO$	3.55
$\kappa[00\bar{1}]$	$Ac_\gamma a_\beta B$	$OT_\downarrow$	$\underline{0.20}$	$Ac_\gamma a_\beta Ba_\gamma a_\alpha C$	$OT_\downarrow:OO$	2.69	$Ac_\gamma a_\beta Ba_\gamma a_\alpha Ca_\beta c_\gamma B$	$OT_\downarrow:OO:OT_\downarrow$	5.37
$\kappa[00\bar{1}]$	$\underline{Ab_\beta a_\gamma C}$	$OT_\downarrow$	$\underline{0.00}$	$\underline{Ab_\beta a_\gamma Ca_\beta a_\alpha B}$	$OT_\downarrow:OO$	$\underline{0.00}$	$Ab_\beta a_\gamma Ca_\beta a_\alpha Ba_\gamma b_\beta C$	$OT_\downarrow O:OO:OT_\downarrow$	4.15
$\kappa[00\bar{1}]$	$Ac_\gamma c_\alpha B$	OO	4.43	$Ac_\gamma c_\alpha Bc_\beta b_\gamma A$	$OO:OT_\downarrow$	2.79	$\underline{Ac_\gamma c_\alpha Bc_\beta b_\gamma Ab_\beta b_\alpha C}$	$OO:OT_\downarrow:OO$	$\underline{0.12}$
$\kappa[00\bar{1}]$	$Ab_\beta b_\alpha C$	OO	2.43	$Ab_\beta b_\alpha Cb_\gamma c_\beta A$	$OO:OT_\downarrow$	1.48	$\underline{Ab_\beta b_\alpha Cb_\gamma c_\beta Ac_\gamma c_\alpha B}$	$OO:OT_\downarrow:OO$	$\underline{0.00}$

TABLE III: Stacking sequence and Al coordination [O for octahedral, T for tetrahedral, with the arrow indicating the direction in which each tetrahedron vertex is pointing: towards the film surface ($\uparrow$) or towards the TiC/film interface ($\downarrow$)] of *unrelaxed* alumina films with $Al_{4n-4}O_{6n}$ stoichiometry and their total energies E_{rel} *after* relaxation (given relative to the structure with lowest total energy for each film thickness). The configurations are grouped together according to the phase and orientation of the alumina bulk structures from which they are derived (left column). Configurations that differ only by a rotation of 180° around TiC[111] are organized into subgroups separated by larger whitespace. In general, the unrelaxed and relaxed atomic structures differ considerably. The stable and potentially metastable (see text for details) configurations are underlined. The *ab initio* study and comparison permit us to make the following set of observations: (i) The unrelaxed configurations with an AC stacking in the first two O layers yield relaxed structures that are in general more favorable than those obtained from configurations in which the stacking sequence has been rotated by 180° around TiC[111] (AB O stacking); (ii) While for the Al_4O_{12} films two different unrelaxed structures lead to the stable configuration, for the other two film thicknesses only one structure leads to the stable configuration; (iii) In general, the stable configurations are obtained from TiC[111]/$\kappa[00\bar{1}]$ initial structures; (iv) The α-type films lead to neither stable nor metastable configurations; and (v) While the stable Al_4O_{12} and Al_8O_{18} films are both obtained from the same unrelaxed interface sequence (same line), the stable $Al_{12}O_{24}$ film derives from another interface sequence.

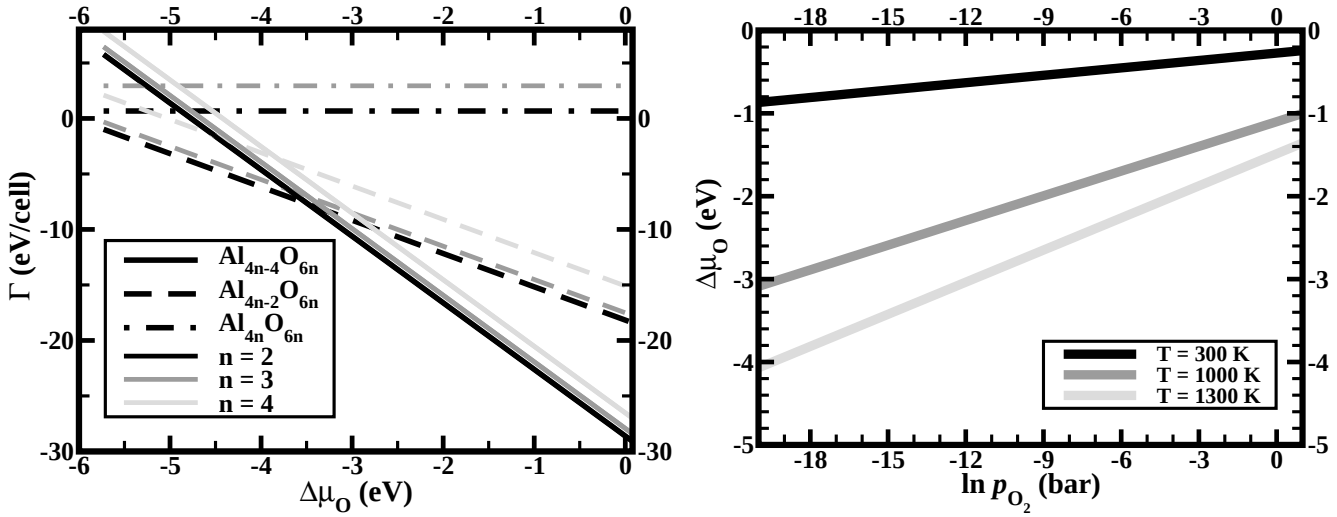

FIG. 3: Thermodynamic stability of thin-film alumina with stoichiometrically different compositions and different thicknesses on the TiC(111) substrate in equilibrium with an O_2 environment. The left panel shows the Gibbs free energy differences Γ (Eq. 12) per unit cell of TiC/thin-film alumina as a function of the O chemical potential $\Delta\mu_O = \mu_O - \frac{1}{2}\epsilon_{O_2}$ (Eq. 13) for all three considered thicknesses and stoichiometric compositions. The left end of each line is defined by the physically allowed range (fcc-Al condensation) of the O chemical potential (Eq. 10). For all thicknesses the alumina films with $Al_{4n-4}O_{6n}$ stoichiometry (solid lines) are stable at medium to high O chemical potential, whereas films with $Al_{4n-2}O_{6n}$ stoichiometry (dashed lines) are stable at low O chemical potential ($\Delta\mu_O < -3.5$ eV). The alumina films with $Al_{4n}O_{6n}$ stoichiometry (dashed-dotted lines) are not stable at any allowed value of the O chemical potential. The right panel shows the O chemical potential $\Delta\mu_O$ as a function of partial O_2 pressure for three different temperatures. We find that a value of $\Delta\mu_O < -3.5$ eV at a temperature $T = 1300$ K corresponds to an O_2 pressure of $P_{O_2} \sim 10^{-15}$ bar.

alumina group	Al_6O_{12} films: alumina stacking	coord. of Al ions	E_{rel} (eV/cell)	$Al_{10}O_{18}$ films: alumina stacking	coord. of Al ions	E_{rel} (eV/cell)	$Al_{14}O_{24}$ films: alumina stacking	coord. of Al ions	E_{rel} (eV/cell)
α	$Ac_3c_2Bc_1$	$OO:O$	0.78	$Ac_3c_2Bc_1c_3Ac_2$	$OO:OO:O$	0.15	$Ac_3c_2Bc_1c_3Ac_2c_1Bc_3$	$OO:OO:OO:O$	0.99
α	$Ab_2b_3Cb_1$	$OO:O$	0.02	$Ab_2b_3Cb_1b_2Ab_3$	$OO:OO:O$	3.22	$Ab_2b_3Cb_1b_2Ab_3b_1Cb_2$	$OO:OO:OO:O$	0.97
$\kappa[001]$	$Ab_\gamma c_\beta Bc_\alpha$	$T_\uparrow O:O$	0.77	$Ab_\gamma c_\beta Bc_\alpha c_\gamma Ab_\gamma$	$T_\uparrow O:OO:O$	1.21	$Ab_\gamma c_\beta Bc_\alpha c_\gamma Ac_\beta b_\gamma Cb_\alpha$	$T_\uparrow O:OO:T_\uparrow O:O$	2.89
$\kappa[001]$	$Ab_\gamma c_\beta Bc_\gamma$	$T_\uparrow O:O$	4.38	$Ab_\gamma c_\beta Bc_\alpha c_\gamma Ac_\beta$	$T_\uparrow O:OO:T_\uparrow$	0.00	$Ab_\gamma c_\beta Bc_\alpha c_\gamma Ac_\beta b_\gamma Cb_\beta$	$T_\uparrow O:OO:T_\uparrow O:O$	2.89
$\kappa[001]$	$Ac_\beta b_\gamma Cb_\alpha$	$T_\uparrow O:O$	0.14	$Ac_\beta b_\gamma Cb_\alpha b_\beta Ac_\beta$	$T_\uparrow O:OO:O$	3.22	$Ac_\beta b_\gamma Cb_\alpha b_\beta Ab_\gamma c_\beta Bc_\alpha$	$T_\uparrow O:OO:T_\uparrow O:O$	2.63
$\kappa[001]$	$Ac_\beta b_\gamma Cb_\beta$	$T_\uparrow O:O$	0.14	$Ac_\beta b_\gamma Cb_\alpha b_\beta Ab_\gamma$	$T_\uparrow O:OO:T_\uparrow$	0.60	$Ac_\beta b_\gamma Cb_\alpha b_\beta Ab_\gamma c_\beta Bc_\gamma$	$T_\uparrow O:OO:T_\uparrow O:O$	2.49
$\kappa[001]$	$Ac_\alpha c_\beta Ba_\beta$	$OO:O$	2.43	$Ac_\alpha c_\beta Bc_\gamma a_\beta Ca_\alpha$	$OO:T_\uparrow O:O$	4.33	$Ac_\alpha c_\beta Bc_\gamma a_\beta Ca_\alpha a_\gamma Bc_\gamma$	$OO:T_\uparrow O:OO:O$	2.34
$\kappa[001]$	$Ac_\alpha c_\beta Bc_\gamma$	$OO:T_\uparrow$	0.80	$Ac_\alpha c_\beta Bc_\gamma a_\beta Ca_\gamma$	$OO:T_\uparrow O:O$	5.05	$Ac_\alpha c_\beta Bc_\gamma a_\beta Ca_\alpha a_\gamma Ba_\beta$	$OO:T_\uparrow O:OO:T_\uparrow$	2.56
$\kappa[001]$	$Ab_\alpha b_\gamma Ca_\gamma$	$OO:O$	2.20	$Ab_\alpha b_\gamma Cb_\beta a_\gamma Ba_\alpha$	$OO:T_\uparrow O:O$	3.86	$Ab_\alpha b_\gamma Cb_\beta a_\gamma Ba_\alpha a_\beta Cb_\beta$	$OO:T_\uparrow O:OO:O$	1.42
$\kappa[001]$	$Ab_\alpha b_\gamma Cb_\beta$ [a]	$OO:T_\uparrow$	0.00	$Ab_\alpha b_\gamma Cb_\beta a_\gamma Ba_\beta$	$OO:T_\uparrow O:O$	4.30	$Ab_\alpha b_\gamma Cb_\beta a_\gamma Ba_\alpha a_\beta Ca_\gamma$	$OO:T_\uparrow O:OO:T_\uparrow$	1.42
$\kappa[00\bar{1}]$	$Ac_\gamma a_\beta Ba_\gamma$	$OT_\downarrow:O$	2.14	$Ac_\gamma a_\beta Ba_\gamma a_\alpha Ca_\beta$	$OT_\downarrow:OO:O$	3.15	$Ac_\gamma a_\beta Ba_\gamma a_\alpha Ca_\beta c_\gamma Bc_\beta$	$OT_\downarrow:OO:T_\downarrow O:O$	0.62
$\kappa[00\bar{1}]$	$Ac_\gamma a_\beta Ba_\alpha$	$OT_\downarrow:O$	1.64	$Ac_\gamma a_\beta Ba_\gamma a_\alpha Cc_\gamma$	$OT_\downarrow:OO:T_\downarrow$	2.25	$Ac_\gamma a_\beta Ba_\gamma a_\alpha Ca_\beta c_\gamma Bc_\alpha$	$OT_\downarrow:OO:OT_\downarrow:O$	0.94
$\kappa[00\bar{1}]$	$Ab_\beta a_\gamma Ca_\beta$	$OT_\downarrow:O$	2.15	$Ab_\beta a_\gamma Ca_\beta a_\alpha Ba_\gamma$	$OT_\downarrow:OO:O$	2.57	$Ab_\beta a_\gamma Ca_\beta a_\alpha Ba_\gamma b_\beta Cb_\alpha$	$OT_\downarrow:OO:T_\downarrow O:O$	0.44
$\kappa[00\bar{1}]$	$Ab_\beta a_\gamma Ca_\alpha$	$OT_\downarrow:O$	1.24	$Ab_\beta a_\gamma Ca_\beta a_\alpha Bb_\beta$	$OT_\downarrow:OO:T_\downarrow$	1.69	$Ab_\beta a_\gamma Ca_\beta a_\alpha Ba_\gamma b_\beta Cb_\gamma$	$OT_\downarrow:OO:T_\downarrow O:O$	1.89
$\kappa[00\bar{1}]$	$Ac_\gamma c_\alpha Bb_\gamma$	$OO:T_\downarrow$	2.36	$Ac_\gamma c_\alpha Bc_\beta b_\gamma Ab_\alpha$	$OO:OT_\downarrow:O$	1.67	$Ac_\gamma c_\alpha Bc_\beta b_\gamma Ab_\beta b_\alpha Cb_\gamma$	$OO:OT_\downarrow:OO:O$	0.00
$\kappa[00\bar{1}]$	$Ac_\gamma c_\alpha Bc_\beta$	$OO:O$	0.80	$Ac_\gamma c_\alpha Bc_\beta b_\gamma Ab_\beta$	$OO:OT_\downarrow:O$	4.84	$Ac_\gamma c_\alpha Bc_\beta b_\gamma Ab_\beta b_\alpha Cc_\beta$	$OO:OT_\downarrow:OO:T_\downarrow$	4.62
$\kappa[00\bar{1}]$	$Ab_\beta b_\alpha Cc_\beta$	$OO:T_\downarrow$	2.17	$Ab_\beta b_\alpha Cb_\gamma c_\beta Ac_\alpha$	$OO:OT_\downarrow:O$	0.37	$Ab_\beta b_\alpha Cb_\gamma c_\beta Ac_\gamma c_\alpha Bc_\beta$	$OO:OT_\downarrow:OO:O$	3.81
$\kappa[00\bar{1}]$	$Ab_\beta b_\alpha Cb_\gamma$ [a]	$OO:O$	0.00	$Ab_\beta b_\alpha Cb_\gamma c_\beta Ac_\gamma$	$OO:OT_\downarrow:O$	3.91	$Ab_\beta b_\alpha Cb_\gamma c_\beta Ac_\gamma c_\alpha Bb_\gamma$	$OO:OT_\downarrow:OO:T_\downarrow$	3.91

[a] The stacking direction ([001] or [00$\bar{1}$]) cannot be inferred at the considered thickness.

TABLE IV: Stacking sequence and Al coordination of *unrelaxed* alumina films with $Al_{4n-2}O_{6n}$ stoichiometry and their relative total-energy differences E_{rel} *after* relaxation. Notation and grouping are the same as in Tab. III. Configurations that differ only in their surface Al ion are grouped together and separated by larger whitespace. The coordination given for the surface Al ion is the one that it would have in the bulk. The *ab initio* study and comparison permit us to make the following set of observations: (i) Although the stable films are generally of κ type, α-type films are competitive, at least for the thinnest films; (ii) For the thinner films, both $\kappa[001]$ and $\kappa[00\bar{1}]$ orientations yield stable and metastable configurations, while for the thicker films, only $\kappa[00\bar{1}]$ leads to (meta-)stable configurations; (iii) The general trend in stability with respect to the O stacking is the same as for the $Al_{4n-4}O_{6n}$ films (*AC* more favorable than *AB*) but with exceptions, in particular, the stable $Al_{10}O_{18}$ and $Al_{14}O_{24}$ configurations originate from structures with *AB* stacking in the first two O layers.

B. Thermodynamical stability

Figure 3 shows our calculated values of Γ for the energetically most favorable configurations of each considered thickness and stoichiometry class. Corresponding values for the potentially metastable configurations can be obtained by adding the relative energies of Tables III–V.

In the physically allowed range of the O chemical potential μ_O (Eq. 10), we find that the stable film belongs to either the $Al_{4n-2}O_{6n}$ or the $Al_{4n-4}O_{6n}$ stoichiometry class, independent of the thickness. The $Al_{4n-4}O_{6n}$ films are stabilized for $\Delta\mu_O \geq -3.5$ eV, whereas for $\Delta\mu_O \leq -3.5$ eV, the $Al_{4n-2}O_{6n}$ films are stable. These findings apply when the films are in equilibrium with an O_2 atmosphere.

In the right panel of Fig. 3 we show the relation between the O chemical potential and the O_2 pressure at several temperatures. We find that an O chemical potential of $\Delta\mu_O \geq -3.5$ eV can only be reached for relatively high temperatures and extremely low O_2 pressures ($T \sim 1300$ K, $p_{O_2} \sim 10^{-15}$ bar (UHV)).

At normal conditions, equilibrium thermodynamics therefore predicts the observation of $Al_{4n-4}O_{6n}$ films.[36] We note that this result is not in contradiction with studies on the α-$Al_2O_3(0001)$ or κ-$Al_2O_3\{001\}$ surfaces, which predict Al termination.[19,32] In our study, the metallic substrate can take or give away charge via the interface, so that the polarity argument that rules out an O-terminated surface of a pure alumina slab cannot be applied to TiC/thin-film alumina.

C. Trends in phase content, orientation, and preferred stacking

It is clear that a detailed analysis of the trends in phase content, orientation, and preferred stacking of the alumina thin films must be based on the relaxed configurations. We find that a classification of thin-film candidate configurations that is based on the unrelaxed structures is dangerous.

The stable and metastable alumina films are in general obtained from truncated TiC/κ-$Al_2O_3[00\bar{1}]$ interface configurations. This would be in agreement with the experimental results that growth of κ-Al_2O_3 is preferred over α-Al_2O_3 on clean TiC(111) substrate.[9] However, truncated TiC/α-Al_2O_3 and TiC/κ-$Al_2O_3[001]$ configu-

alumina group	alumina stacking	coord. of Al ions	$E_{\rm rel}$ (eV/cell)
		Al_8O_{12} films	
α	$Ac_3c_2Bc_1c_3$	$OO:OO$	2.46
α	$Ab_2b_3Cb_1b_2$	$OO:OO$	1.92
$\kappa[001]$	$Ab_\gamma c_\beta Bc_\alpha c_\gamma$	$T_\uparrow O:OO$	3.17
$\kappa[001]$	$Ac_\beta b_\gamma Cb_\alpha b_\beta$	$T_\uparrow O:OO$	2.57
$\kappa[001]$	$Ac_\alpha c_\beta Bc_\gamma a_\beta$	$OO:T_\uparrow O$	4.07
$\kappa[001]$	$Ab_\alpha b_\gamma Cb_\beta a_\gamma$	$OO:T_\uparrow O$	2.06
$\kappa[00\bar{1}]$	$Ac_\gamma a_\beta Ba_\gamma a_\alpha$	$OT_\downarrow:OO$	2.08
$\kappa[00\bar{1}]$	$Ab_\beta a_\gamma Ca_\alpha a_\beta$	$OT_\downarrow:OO$	0.00
$\kappa[00\bar{1}]$	$Ac_\gamma c_\alpha Bc_\beta b_\gamma$	$OO:OT_\downarrow$	2.90
$\kappa[00\bar{1}]$	$Ab_\beta b_\alpha Cb_\gamma c_\beta$	$OO:OT_\downarrow$	1.80
		$Al_{12}O_{18}$ films	
α	$Ac_3c_2Bc_1c_3Ac_2c_1$	$OO:OO:OO$	2.88
α	$Ab_2b_3Cb_1b_2Ab_3b_1$	$OO:OO:OO$	3.93
$\kappa[001]$	$Ab_\gamma c_\beta Bc_\alpha c_\gamma Ac_\beta b_\gamma$	$T_\uparrow O:OO:T_\uparrow O$	1.42
$\kappa[001]$	$Ac_\beta b_\gamma Cb_\alpha b_\beta Ab_\gamma c_\beta$	$T_\uparrow O:OO:T_\uparrow O$	1.16
$\kappa[001]$	$Ac_\alpha c_\beta Bc_\gamma a_\beta Ca_\alpha a_\gamma$	$OO:T_\uparrow O:OO$	2.78
$\kappa[001]$	$Ab_\alpha b_\gamma Cb_\beta a_\gamma Ba_\alpha a_\beta$	$OO:T_\uparrow O:OO$	1.48
$\kappa[00\bar{1}]$	$Ac_\gamma a_\beta Ba_\gamma a_\alpha Ca_\beta c_\gamma$	$OT_\downarrow:OO:OT_\downarrow$	0.49
$\kappa[00\bar{1}]$	$Ab_\beta a_\gamma Ca_\beta a_\alpha Ba_\gamma b_\beta$	$OT_\downarrow:OO:OT_\downarrow$	0.00
$\kappa[00\bar{1}]$	$Ac_\gamma c_\alpha Bc_\beta b_\gamma Ab_\beta b_\alpha$	$OO:OT_\downarrow:OO$	1.72
$\kappa[00\bar{1}]$	$Ab_\beta b_\alpha Cb_\gamma c_\beta Ac_\gamma c_\alpha$	$OO:OT_\downarrow:OO$	0.52

TABLE V: Stacking sequence and Al coordination of the *unrelaxed* alumina films with $Al_{4n}O_{6n}$ stoichiometry and their relative total-energy differences $E_{\rm rel}$ *after* relaxation. Notation and grouping are the same as in Tab. III. The *ab initio* study and comparison permit a number of observations that are similar to those we made for the $Al_{4n-4}O_{6n}$ films (Tab. III). However, the $Al_{4n}O_{6n}$ films are thermodynamically unstable, see Sec. V B.

rations are (meta-)stable in the case of the thinner films with $Al_{4n-2}O_{6n}$ stoichiometry.

Comparing configurations that are derived from structures that differ only by a reflection about the yz-plane, we notice that, generally, the unrelaxed structure with AC stacking in the bottom two O layers yield more favorable configurations than the structures with AB stacking. There are, however, exceptions; in particular the energetically most favorable $Al_{10}O_{18}$ film and each one of the potentially metastable $Al_{10}O_{18}$ and $Al_{14}O_{24}$ films posses an AB stacking in the bottom two O layers. We also note that, in general, the detailed stacking sequence of the energetically most favorable configurations varies strongly with the film thickness.

In summary, although there are some general stability trends that can be inferred from the phase content, orientation, and stacking of the unrelaxed thin-film configurations, there are also several noticeable exceptions. In particular the $Al_{4n-2}O_{6n}$ films tend to break the rules.

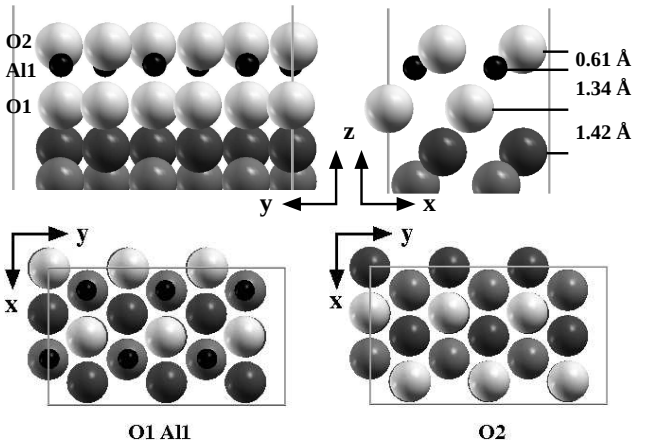

FIG. 4: Atomic structure of the stable Al_6O_{12} film. The color coding is: Dark gray = Ti, light gray = C, light = O, and black = Al. The top panel shows the projected side views along [100] and [010] including interlayer distances. The bottom panel shows the top views on the atomic layers [as defined in the top panel]. The Al coordination is OOO (O: octahedral, T: tetrahedral). Note that the film is O terminated after relaxation.

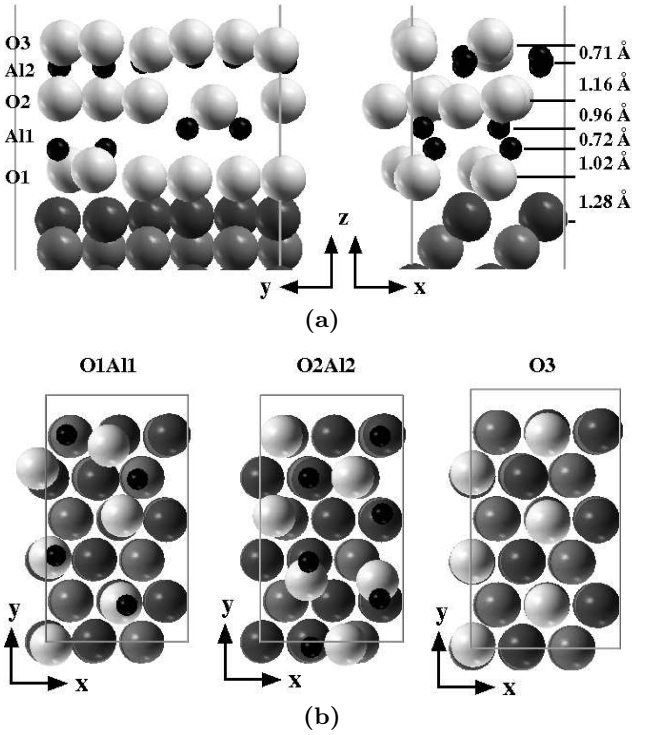

FIG. 5: Atomic structure of the stable $Al_{10}O_{18}$ film (color coding as in Fig. 4). The film is O terminated after relaxation. The Al coordination is $T_\downarrow T_\uparrow : T_\downarrow OO$ (O: octahedral, T: tetrahedral, the arrows indicate the direction in which the tetrahedra point, different Al layers are separated by ':'). Note that tetrahedral coordination dominates and that both Al pairs in the bottom layer are tetrahedrally coordinated, with tetrahedra pointing in opposite directions ($T_\uparrow T_\downarrow$).

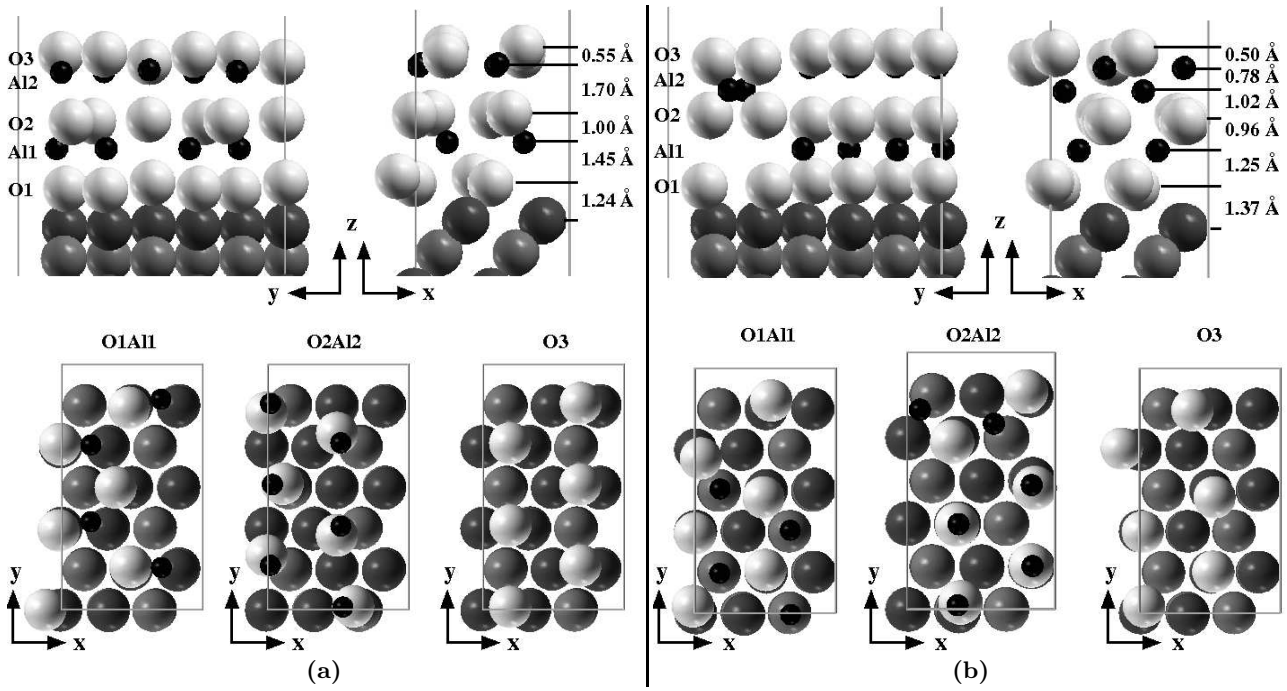

FIG. 6: Atomic structure of the two potentially metastable $Al_{10}O_{18}$ films. Color coding and notation are as in Fig. 4. The Al coordinations are (a) $OO:T_{\downarrow}T_{\downarrow}T_{\downarrow}$ and (b) $OO:T_{\downarrow}T_{\downarrow}O$ (O: octahedral, T: tetrahedral, the arrows indicate the direction in which the tetrahedra point, different Al layers are separated by ':').

VI. RESULTS II: ATOMIC STRUCTURE OF STABLE AND METASTABLE FILMS

In this section we analyze in detail the atomic structure of the relaxed alumina films with $Al_{4n-2}O_{6n}$ and $Al_{4n-4}O_{6n}$ stoichiometries that are found to be stable and potentially metastable in our implementation of the proposed method for structure search. While a number of structural motifs that were included in the initial candidate set are preserved, also novel motifs that strongly deviate from those in the bulk phase are identified. Both preserved and novel motifs together, give insight into structural motifs of more accurate thin-film candidates.

A. Atomic structure of the $Al_{4n-2}O_{6n}$ films

Two-O-layer thick films – Al_6O_{12}. Figure 4 shows the atomic structure of the energetically most favorable Al_6O_{12}. It corresponds to a close-packed continuation of the TiC ABC substrate stacking, that is, the alumina stacking is $Ab_{\alpha}b_{\beta}b_{\gamma}C$. All Al ions share the same atomic plane and are octahedrally (O) coordinated. The relaxed film is O terminated. Compared to TiC/O [O monolayer on TiC(111)], the Ti–O layer separation is drastically increased (+0.5 Å).

The potentially metastable Al_6O_{12} structures possess almost the same structure as the energetically most favorable one. They differ only by a slight displacement along the z direction of some of the Al ions.

Three-O-layer thick films – $Al_{10}O_{18}$. Figure 5 shows the atomic structure of the energetically most favorable $Al_{10}O_{18}$ film. Potentially metastable configurations are displayed in Fig. 6. In all cases, the Ti–O layer separation is shorter than in the energetically most favorable Al_6O_{12} film, but still considerably larger than in TiC/O ($\sim$ +0.3 Å). We also note that in the stable $Al_{10}O_{18}$ film, two of the six O ions in the bottom O layer are slightly lifted off from the TiC substrate. In the potentially metastable films, no O ion is lifted off.

In all displayed films, the surface Al pairs have relaxed below the terminating O layer, so that the second Al layer consists of three Al pairs and the film is O terminated.

The stacking of O layers is approximately described by ABA, $AB(AC)_{\rm bridge}$, and ACA for the energetically most favorable film and the two potentially metastable films respectively. The order is only approximate because a number of O ions are significantly distorted from ideal sites (as defined by the underlying TiC substrate). They are often located in bridge or cusp sites. This effect is most pronounced in the third O layer in the first potentially metastable film, which is entirely located in bridge sites.

Similarly, the Al ions often deviate from ideal sites so that their description in terms of the bulk stacking labels becomes cumbersome. However, these distortions always occur pairwise, that is, Al pairs that are related by a bulk stacking label are dislocated symmetrically. The candidate structures generally preserve this symmetry of

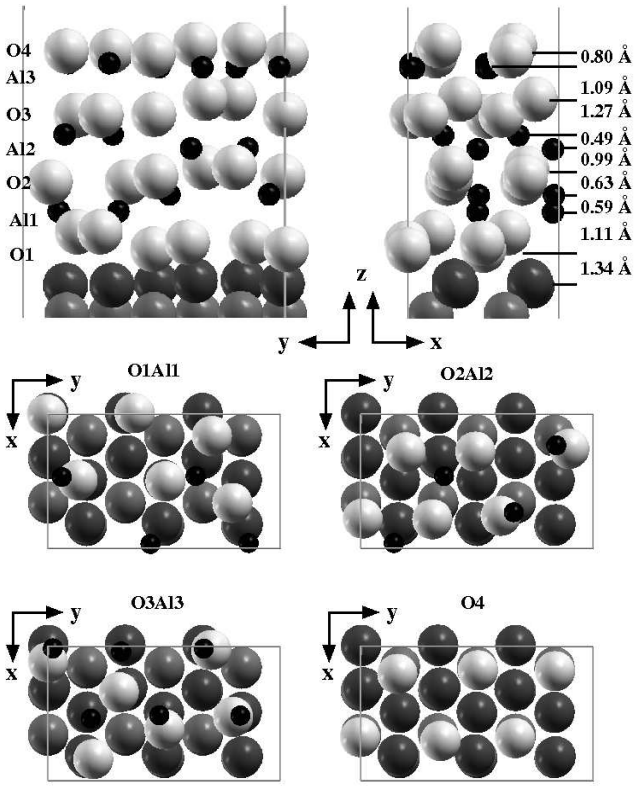

FIG. 7: Atomic structure of the stable $Al_{14}O_{24}$ film (color coding and notation as in Fig. 4). The film is O terminated after relaxation. The Al coordination is $OT_\downarrow : T_\uparrow T_\downarrow : OT_\downarrow T_\downarrow$ (O: octahedral, T: tetrahedral, the arrows indicate the direction in which the tetrahedra point, different Al layers are separated by ':'). As in the most favorable $Al_{10}O_{18}$ film, there is a layer in which both Al pairs are tetrahedrally coordinated, with tetrahedra pointing in opposite directions ($T_\downarrow T_\uparrow$). Here, they are located in the second Al layer.

the motifs of the bulk phases.

The coordination of the Al ions is described as $T_\uparrow T_\downarrow : T_\downarrow OO$, $OO : T_\downarrow T_\downarrow T_\downarrow$ and $OO : OT_\downarrow T_\downarrow$, for the energetically most favorable and the two metastable films respectively. Here and in the following O denotes octahedrally coordinated Al pairs, T tetrahedrally coordinated pairs. For tetrahedral coordination, $T_\uparrow$ means that the tetrahedra point along the TiC[111] direction, away from the interface, whereas $T_\downarrow$ indicates that they point towards the interface. Different Al layers are separated by ':'.

We notice that in all configurations, there is a large number of tetrahedrally coordinated Al ions (40-60%) and these can share the same atomic layer. In particular a larger number of tetrahedrally coordinated Al ions is favored. Furthermore, the energetically most favorable film contains tetrahedrally coordinated Al ions that share one layer and for which the tetrahedra point into opposite directions.

Four-O-layer thick films – $Al_{14}O_{24}$. Figures 7 and 8 show the atomic structure of the energetically most favorable film and the two potentially metastable $Al_{14}O_{24}$ films, respectively. The Ti–O layer separations are comparable to those in the energetically favorable $Al_{10}O_{18}$ films. Also, in the stable $Al_{14}O_{24}$ film, two of the six O ions in the bottom O layer are slightly lifted off from the TiC substrate, whereas this is not observed in the potentially metastable films. In the most favorable film, the surface Al pairs have relaxed below the terminating O layer, so that the second Al layer consists of three Al pairs and the film is O terminated. However, both potentially metastable films are Al terminated even after relaxations.

The stacking of O layers is more strongly distorted as in the case of $Al_{10}O_{18}$ films, in particular in the most favorable film. From the figures, we find the approximate O stacking sequences $A(BC)_{\rm bridge}(A_\alpha A_\gamma C_\beta)B$ [most favorable film Fig. 7], $ACBC$ [first potentially metastable, Fig. 8.(a)], and $ABAC$ [second potentially metastable film, Fig. 8.(b)], where we use the the labeling (subscript) of the Al positions also for O ions and note that some of the ions are in fact dislocated from ideal sites.

The Al ions are distorted correspondingly. This distortion is again pairwise and symmetrically for the energetically most favorbale and the first potentially metastable films. For the second potentially metastable film, this is not true. Both on the surface and in the first and second layer below the surface there are Al ions that have relaxed in a non-symmetric way.

The coordination of the Al ions is given by $OT_\downarrow : T_\downarrow T_\uparrow : OT_\downarrow T_\downarrow$ (most favorable), $OT_\downarrow : OO : OT_\downarrow$ (first potentially metastable), and $T_\downarrow T_\downarrow : oT_\downarrow t_\downarrow : ooT_\downarrow$ (second potentially metastable). In the last sequence, the coordination of single ions that do not belong to a pair is denoted by small letters (t, o). Also, the coordination of the surface Al ions is not given for the two potentially metastable films.

The result is similar to that for the $Al_{14}O_{24}$ films. In general, a large number of tetrahedrally coordinated Al ions is favored. In the most favorable film 70% of the Al ions are tetrahedrally coordinated. Furthermore, there is a layer with purely tetrahedrally Al ions and tetrahedra pointing into opposite directions (second Al layer). The first potentially metastable film possesses only 30% tetrahedrally coordinated Al ions. Inspection of the detailed stacking sequence, $Ab_\beta a_\gamma C a_\alpha a_\beta B b_\beta a_\gamma C b_\alpha$, identifies this structure as a partial κ-Al_2O_3 configuration with an orientation TiC[111]/$\kappa[00\bar{1}]$.

B. Atomic structure of the $Al_{4n-4}O_{6n}$ films

In general the potentially metastable $Al_{4n-4}O_{6n}$ films (if present) possess the same atomic structure as the the energetically most favorable film but rotated by 180° around the TiC[111] direction [$B \leftrightarrow C, \beta(2) \leftrightarrow \gamma(3)$]. They are therefore not discussed in the following.

Two-O-layer thick films – Al_4O_{12}. Figure 9 reports the calculated atomic structure of the energetically most favorable Al_4O_{12} film. It is noticeable that the O–O sep-

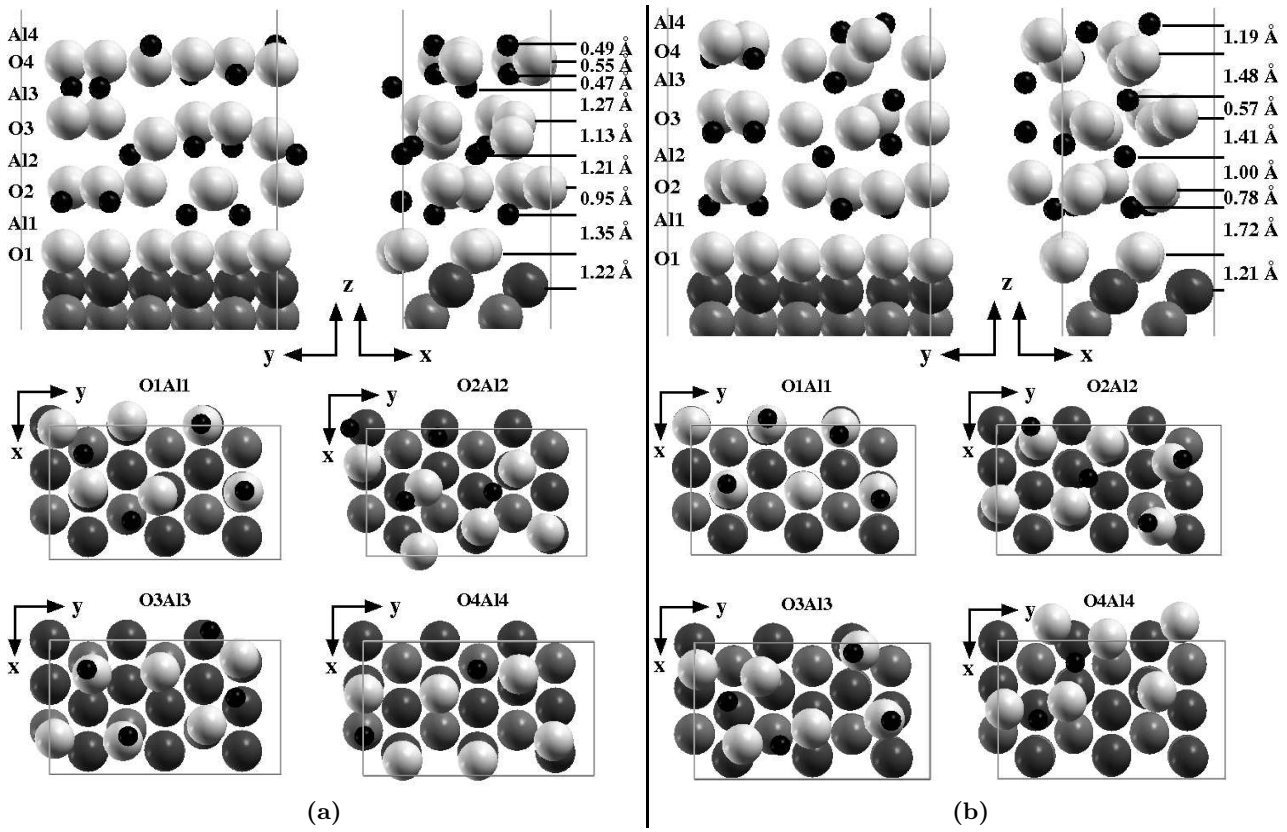

FIG. 8: Atomic structure of the potentially metastable $Al_{14}O_{24}$ films. Color coding and notation are as in Fig. 4. The films are Al terminated even after relaxations. The Al coordinations are (without surface Al) (a) $OT_\downarrow : OO : T_\downarrow O$, (b) $T_\downarrow T_\downarrow : T_\downarrow(t_\downarrow o) : T_\downarrow O$ (O: octahedral, T: tetrahedral, t single tetrahedral Al ion, o single octahedral Al ion, the arrows indicate the direction in which the tetrahedra point).

aration in the alumina is relatively large, $d_{\text{O-O}} \sim 2.6$ Å on average, and that the two Al pairs are not located between the O layers but are almost incorporated in the surface O layer, which leads to a large splitting of that layer. At the same time, the Ti–O separation is comparably small and equals that in TiC/O.

Hence, although predicted to be stable in a thermodynamical sense, structurally this TiC/Al_4O_{12} configuration separates into a $TiC/O/Al_4O_6$ system, that is, a strongly bonded O monolayer on the TiC substrate with a thin alumina overlayer on top.

The stacking of the O layers is AC, and the coordination of the Al ions approx $T_\downarrow O$.

Three-O-layer thick films – Al_8O_{18}. Figure 10 shows the atomic structure of the energetically most favorable Al_8O_{18} film. The average O–O separation between the bottom two O layers is $d_{\text{O-O}} \sim 2.5$ Å, which is slightly shorter than the one in the stable Al_4O_{12} film. At the same time, the Ti–O separation is increased to 1.15 Å.

The stacking of the O layers is approximately ACA. In the middle O layer, the two O ions that should be located in C_β are, however, dislocated to cusp sites. Furthermore the whole surface O layer is strongly distorted from ideal sites. The coordination sequence of the Al ions is $T_\downarrow : OT_\downarrow T_\downarrow$.

Only one of the original two Al pairs is left between the bottom two O layers after relaxation, the other pair moving in between the top two O layers. Interestingly, one of the interfacial Ti atoms has left the Ti layer and relaxed slightly in between the bottom two O layers. Again, structurally the TiC/Al_8O_{18} configuration appears as a partially decoupled $TiC/O/Al_8O_{12}$ system. Here, however, the Ti impurity above the bottom O layer may be a stabilizing factor.

Four-O-layer thick films – $Al_{12}O_{24}$. In Fig. 11, we show the atomic structure of the stable $Al_{12}O_{24}$ film. The O stacking is $ACAB$ and hardly distorted. All Al ions have octahedral coordination. Thus, the present structure mixes the O stacking of bulk κ-Al_2O_3 with the Al coordination of bulk α-Al_2O_3.

The O–O separation $d_{\text{O-O}} \sim 2.5$ Å is again very large and the Ti–O separation is TiC/O like. Also, one of the original two Al pairs in the bottom Al layer has relaxed upward through the middle Al layer and into the top layer. The other Al pair of the bottom layer is after relaxation located only 0.1 Å below the middle O layer. Consequently, also the $TiC/Al_{12}O_{24}$ configuration can again be considered as a decoupled, weakly binding $TiC/O/Al_{12}O_{18}$ system.

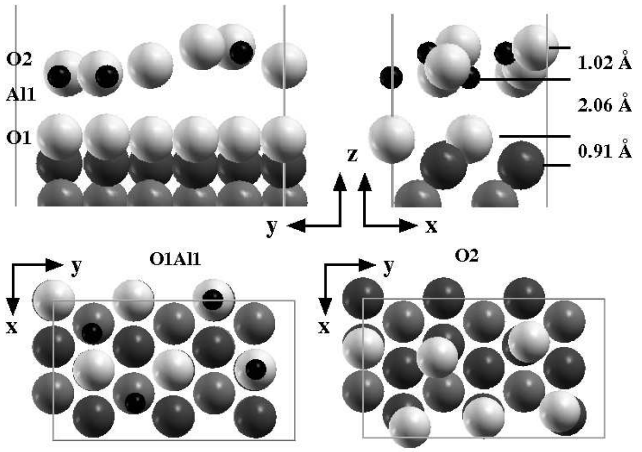

FIG. 9: Atomic structure of the stable Al_4O_{12} film (color coding and notation as in Fig. 4). Note the large O–O interlayer distance, which forms an almost empty region in between the two O layers. As a consequence, the TiC/alumina system separates into TiC/O/alumina. The Al coordination is $T_\downarrow O$ (O: octahedral, T: tetrahedral, the arrow indicates the direction in which the tetrahedra point).

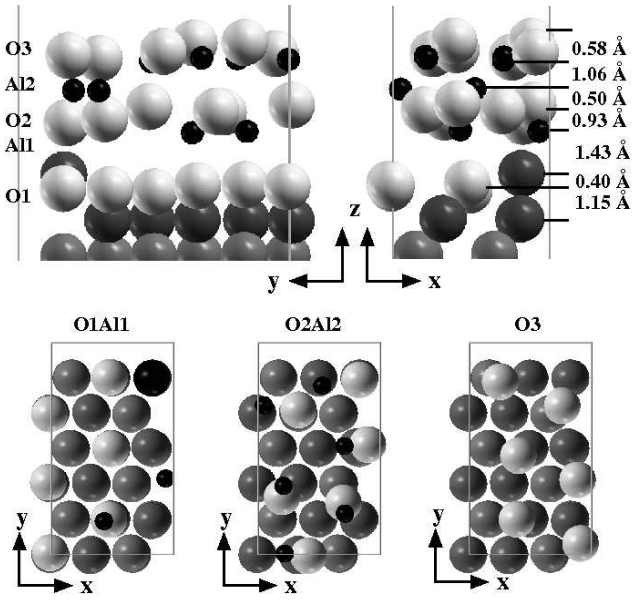

FIG. 10: Atomic structure of the stable Al_8O_{18} film (color coding and notation as in Fig. 4). Note that one of interfacial Ti atoms has relaxed to a position slightly above the bottom O layer. In the top view on O1Al1 in the lower panel, this Ti impurity is indicated by the large black ball. The Ti impurity may strengthen the TiC–alumina bond. The Al coordination is $T_\downarrow : OT_\downarrow T_\downarrow$ (O: octahedral, T: tetrahedral, the arrows indicate the direction in which the tetrahedra point).

VII. DISCUSSION

A. Thin-film structure search method

Although the relations between unrelaxed alumina structures and their energies after relaxations show some general trends, see Sec. V C, several important exceptions occur. In particular, these exceptions can result into the energetically most favorable structure.

These exceptions illustrate a potential danger of applying simple MC methods to the problem of finding the stable thin-film oxide structures. An importance sampling of the thin-film configuration space based on a classification of the unrelaxed structures in terms of, for instance, alumina phase content, orientation, and/or O stacking may easily miss such exceptions.

In our analysis of the relaxed atomic structure, we find that (apart from one possibly metastable $Al_{12}O_{24}$ film) none of the stable and potentially metastable films shows a partial bulk alumina structure. Nevertheless in all structures the Al ions still obey parts of the bulk symmetry. In particular, the positions of the Al pairs in the relaxed films are still pairwise related by the mapping given in Fig. 1.

The set of thin-film candidates does have new structure motifs different from those found in the bulk phases. The thin-film relaxation causes differences the coordination of the Al pairs and/or in the stacking sequence of the O planes. For the $Al_{4n-2}O_{6n}$ films we find that (i) layers with only tetrahedrally coordinated Al ions, $T_\downarrow T_\uparrow$ or $T_\downarrow T_\downarrow$, are energetically favorable; (ii) layers with only octahedrally coordinated Al ions are present in both stable and metastable films; (iii) Al layers with coordination $T_\uparrow T_\uparrow$ are not present. For the $Al_{4n-4}O_{6n}$ films we find essentially only Al coordinations of the types OO and $OT_\downarrow$. The $T_\downarrow T_\downarrow O$ coordination of the Al layer directly below the surface O layer of the stable Al_8O_{18} film should be considered as a surface effect. The absence of $OT_\uparrow$ is consistent with the fact that the stable configurations all derive from TiC/$\kappa[00\bar{1}]$ sequences. However, the relaxed configurations are still not conform with the bulk stacking. In particular, for the stable $Al_{12}O_{24}$ film, we observe only octahedrally coordinated Al ions in combination with an $ACAB$ stacking.

The finding of new structure motifs, not explicitly included in the network of initial configurations, implies a significant strength. It shows that the proposed method is not restricted to a sorting of the original candidate structures in an energetic order, but that it is indeed capable to predict energetically more favorable film geometries than what strictly constitutes symmetries in partial bulk structures.

The identification of candidates for stable and metastable thin-film structures with some novel structural motifs also suggests how the candidate space and the search could be broadened in a cost-efficient approach. A broadening of the network of initial thin-film configurations can be made in the scope of structural elements. It would include motifs found in the bulk α- and κ-Al_2O_3 but with a different weighting in choice of coordination for Al ions. In particular, the positions of the Al ions are still related pairwise, which restricts any

n (# of O layers)	Favorable O stacking and Al coordination	
	$Al_{4n-2}O_{6n}$	$Al_{4n-4}O_{6n}$
2	O_A Al^O Al^O Al^O O_C	O_A Al^O $Al^{T\downarrow}$ O_C
3	O_A $Al^{T\uparrow}$ $Al^{T\downarrow}$ O_B Al^O $Al^{T\downarrow}$ Al^O O_A O_A Al^O Al^O O_C $Al^{T\downarrow}$ $Al^{T\downarrow}$ $Al^{T\downarrow}$ O_A O_A Al^O Al^O O_C Al^O $Al^{T\downarrow}$ $Al^{T\downarrow}$ O_A	O_A $Al^{T\downarrow}$ O_C Al^O $Al^{T\downarrow}$ $Al^{T\downarrow}$ O_B
4	O_A Al^O $Al^{T\downarrow}$ O_B $Al^{T\uparrow}$ $Al^{T\downarrow}$ O_A Al^O $Al^{T\downarrow}$ $Al^{T\downarrow}$ O_C O_A Al^O $Al^{T\downarrow}$ O_C Al^O Al^O O_B Al^O $Al^{T\downarrow}$ O_C Al	O_A Al^O O_C Al^O Al^O O_A Al^O Al^O Al^O O_B

TABLE VI: Favorable structural motifs for relaxed films of different thicknesses. The label of the O layers indicate the approximate location of that layer with respect to the substrate surface (A = fcc, B = hcp, and C = top). The label of the Al pairs indicate their approximate coordination (O: octahedral, T: tetrahedral, the arrows indicate the direction in which the tetrahedra point).

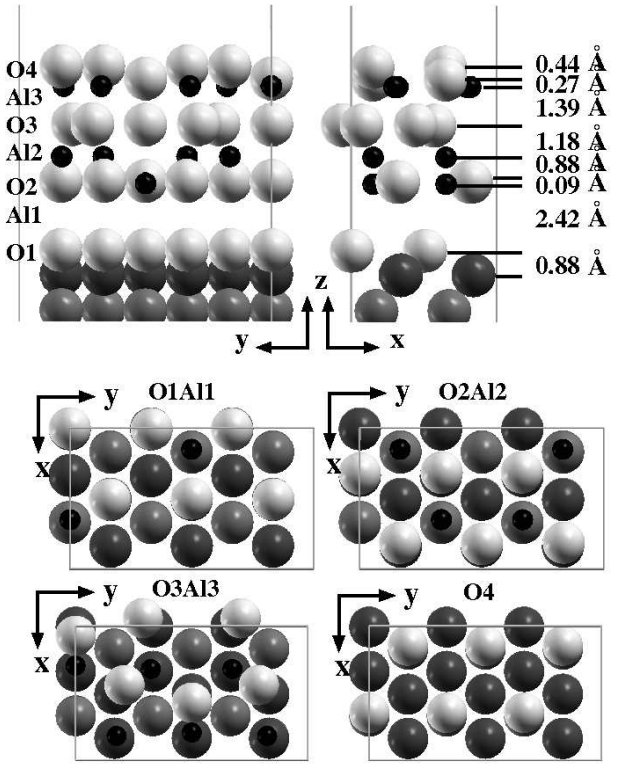

FIG. 11: Atomic structure of the stable $Al_{12}O_{24}$ film (color coding and notation as in Fig. 4). Note again the large interlayer distance between the bottom two O layers. The absence of Al ions in between these O layers strongly indicates that the TiC/alumina system separates into weakly bound TiC/O/alumina. The Al coordination is $O : OO : OOO$, *i.e.*, purely octahedral.

broadening of the network of necessary initial thin-film configurations very significantly. We find indications for a significant increase in preference for tetrahedral coordination of Al ions in the thin-film candidates. This motif is included in the initial thin-film network (which has many structures derived from κ-Al_2O_3). However, a natural further refinement of the present implementation of the proposed search method would be to include initial structures with a higher degree of tetrahedral coordination of Al ions. It is possible to cast this broadening of the initial network into the framework of a genetic algorithm for identifying surface reconstructions.[37,38,39]

We emphasize that a future, extended search for thin-film candidates is not expected to affect conclusions concerning thermodynamical stability of the various classes of ultra-thin alumina films. Since the slopes of Γ in Figs. 3 will remain unchanged, finding possibly energetically more favorable structures in the two relevant stoichiometry classes will only resize the regions in which the different stoichiometries are stabilized. To make the $Al_{4n-4}O_{6n}$ films generally unstable in comparison to $Al_{4n-2}O_{6n}$ films, the truly stable $Al_{4n-2}O_{6n}$ configuration needs to gain at least ~ 10 eV compared to the stable $Al_{4n-4}O_{6n}$ found here.

B. Note on the stability of CVD TiC/alumina wear-resistant coatings

We emphasize that our results on the thermodynamical stability of thin-film alumina on TiC are critically based on the assumption of thermal equilibrium between the films and an O_2 environment. The finding that the preferred structure is described as a $TiC/O/Al_{4(n-1)}O_{6(n-1)}$ system (after relaxations) with a weak binding[40] between TiC/O and $Al_{4(n-1)}O_{6(n-1)}$ is not in contradiction with the required exceptionally strong binding in a wear-resistant coating application. It rather shows that equilibrium between O_2 and oxygen in the alumina during CVD growth of alumina is not reached. At environmental conditions relevant for CVD growth, as will be be discussed in a forthcoming paper,[41] we find that it is instead the Al terminated films that are stabilized.

VIII. CONCLUSIONS

We present a method to sample the configuration space of possible thin-film structures of complex oxides on a substrate. A well-defined network of initial configurations for promising thin-film candidates can be designed

from the oxide bulk structure. *Ab initio* calculations of relaxation deformations provide candidates for thin films as a function of stoichiometry and oxygen-layer thickness.

The method has been illustrated for TiC/thin-film alumina, where experimental evidence[9,10] can be used to reduce the network of initial thin films to contain structural motifs defined by bulk α- and κ-Al_2O_3. Based on this assumption, we have determined structural elements in and candidates for the energetically most favorable (stable or potentially metastable) TiC/thin-film alumina configurations for three thicknesses and three stoichiometry classes.

Our method for *ab initio* search and study of thin-film structures has predictive power and provides detailed insight into the nature and atomic structure of thin-film alumina on TiC. The structures that are predicted by our method differ in their motifs heavily from motifs of the bulk structures, in particular in terms of the Al coordination. In principle, this warns that the present implementation of the search may not yet be complete and that we cannot make an authoritative prediction of the stable thin-film alumina structure; we can at present only identify key structural elements. More importantly, this finding of additional favorable motifs documents predictive power. It shows that the search method can identify candidates with a nature that is not explicitly included in the network of initial configurations.

The different stoichiometry classes have been compared by means of Gibbs free energies. Assuming equilibrium with an O_2 environment, we find that for the considered thicknesses of two, three, or four O layers (corresponding to $n = 2$, 3, or 4, respectively) the stable films are either those with $Al_{4n-4}O_{6n}$ stoichiometry (for medium to high O chemical potentials) or those with $Al_{4n-2}O_{6n}$ stoichiometry (for very low O chemical potentials). The films with $Al_{4n}O_{6n}$ stoichiometry are never stabilized.

Acknowledgments

The authors thank Sead Canovic and Mats Halvarsson for useful discussions. Support from the Swedish National Graduate School in Materials Science, from the Swedish Foundation for Strategic Research (SSF) through ATOMICS, from the Swedish Research Council (VR), and from the Swedish National Infrastructure for Computing (SNIC) are gratefully acknowledged.

---

* Electronic address: rohrer@chalmers.se

1. α-,γ-, δ-, θ-, κ-Al_2O_3, ..., see *e.g.* I. Levin and D. Brandon, J. Am. Ceram. Soc. **81**, 1995 (1998).
2. rutile-, anatase-, brookite, and columbite (α-PbO_2) TiO2, and Ti_2O_3, see *e.g.* J. Haines and J. M. Leger, Physica B, **192**, 233 (1993); J. K. Dewhurst and J. E. Lowther, Phys. Rev. B 54, R3673 (1996).
3. VO_x (rocksalt), VO_2 (rutile), V_2O_3 (corundum), V_2O_5 (orthorhombic), see *e.g.* S. Surnev, M. G. Ramsey and F. P. Netze, Prog. Surf. Sci. **73**, 117 (2003).
4. cubic, tetragonal, and monoclinic modifications of HfO_2, see *e.g.* J. Wang, H. P. Li and R. Stevens, J. Mat. Sci. **27**, 5397 (1992).
5. A. Stierle *et al.*, Science **303**, 1652 (2004).
6. G. Kresse *et al.*, Science **308**, 1440 (2005).
7. S. Canovic *et al.*, Surf. Coat. Technol. **202**, 522 (2007).
8. M. Halvarsson *et al.*, J. Phys.: Conf. Ser. **126**, 012075 (2008) .
9. M. Halvarsson, H. Nordén, and S. Vuorinen, Surf. Coat. Technol. **61**, 177 (1993).
10. M. Halvarsson, J.E. Trancik, and S. Ruppi, Int. J. Refract. Met. Hard Mater. **23**, 32 (2006).
11. J. Rohrer *et al.*, J. Phys.: Conf. Ser. **100**, 082010 (2008)
12. Both alumina phases, in particular κ-Al_2O_3, yield a huge number of possible thin-film configurations. The primitive unit cell of κ-Al_2O_3, with its $ABAC$ stacking of O planes along the [001] direction, see also Fig. 1, allows for $\binom{18}{4} = 3060$ combinatorially possible distributions of the four Al ions within each atomic plane. Use of symmetry and electrostatics arguments (for example, no occupation of nearest-neighbor sites for Al), reduces this number to 222. However, it is clear that for thin films of a few atomic layers, the number of possible atomic structures increases rapidly.
13. R. Car and M. Parrinello, Phys. Rev. Lett. **55**, 2471 (1985).
14. E. Kaxiras *et al.*, Phys. Rev. B *35*, 9625 (1987).
15. I. G. Batyrev, A. Alavi, and M. W. Finnis, Phys. Rev. B **62**, 4698 (2000).
16. K. Reuter and M. Scheffler, Phys. Rev. B **65**, 035406 (2001).
17. L. Pauling and S. B. Hendricks, J. Am. Chem. Soc. **47**, 781 (1925); M. L. Kronberg, Acta Metall. **5**, 507 (1957); W. E. Lee and K. P. D. Lagerlof, J. Electron. Microc. Tech. **2**, 247 (1985).
18. Y. Yourdshahyan *et al.*, J. Am. Ceram. Soc. **82**, 1365 (1999).
19. C. Ruberto, Y. Yourdshahyan, and B. I. Lundqvist, Phys. Rev. B **67**, 195412 (2003).
20. W. E. Lee and K. P. D. Lagerlof, J. Electron. Microc. Tech. **2**, 247 (1985).
21. M. Halvarsson, V. Langer, S. Vuorinen, Surf. Coat. Technol. **76-77**, 358 (1995).
22. M. Halvarsson, Ph. D. Thesis, Chalmers University of Technology (1994).
23. C. Ruberto and B. I. Lundqvist, Phys. Rev. B **75**, 235438 (2007); A. Vojvodic, C. Ruberto, and B. I. Lundqvist, Surf. Sci. **600**, 3619 (2006).
24. A. Dunand, H. D. Flack and K. Yvon, Phys. Rev. B **31**, 2299 (1985).
25. C. Oshima *et al.*J. Less-Common Met. 82, p. 69 (1981).
26. S. Canovic *et al.*, Surf. Coat. Technol. **202** 522 (2007).
27. dacapo, *https://wiki.fysik.dtu.dk/dacapo.*
28. D. Vanderbilt, Phys. Rev. B **41**, 7892 (1990).
29. J. P. Perdew *et al.*, Phys. Rev. B **46**, 6671 (1992).

[30] H. J. Monkhorst and J. D. Pack, Phys. Rev. B **13**, 5188 (1976).
[31] C. Ruberto, Ph. D. Thesis, Chalmers University of Technology (2001).
[32] X.-G. Wang, A. Chaka, and M. Scheffler, Phys. Rev. Lett. **84**, 3650 (2000); A. Marmier and S. C. Parker, Phys. Rev. B **69**, 115409 (2004).
[33] W. Zhang, J. R. Smith, and X.-G. Wang, Phys. Rev. B **70**, 024103 (2004).
[34] Note that, even in the absense of δ vibrational contributions are of minor relevance: First, our results found by excluding $\Gamma^{\rm vib}$ show that the in differences Γ for different stoichiometric film compositions are of the order of $5-10$ eV in the largest range of most interesting region of the O chemical potential. Second, although small regions were these differences become of the order of $\Gamma^{\rm vib}$ exist we have to keep in mind that it is not the absolute value of $\Gamma^{\rm vib}$ but rather the differences in $\Gamma^{\rm vib}$ for different surface terminations that determine the stability. These can be expected to be considerably smaller than the absolute value of $\Gamma^{\rm vib}$. Hence, the only effect of neglecting vibrational contributions is a small uncertainty in the value of $\mu_{\rm O}$ which divides regions where different stoichiometries are stable.
[35] NIST-JANAF Thermochemical Tables 4$^{\rm th}$ Ed., Malcom W. Chase Jr. (1998).
[36] By including a thickness and stoichiometry dependent value of δ we find that the $Al_{4n-4}O_{6n}$ films are still stabilized down to $\mu_{\rm O} \geq -2$ to -2.5 eV, where the higher value applies for the thickest and the lower for the thinnest films. An O chemical potential of $\Delta\mu_{\rm O} \geq -2$ eV, is reached for considerably higher O_2 pressures (*e.g.* $T \sim 1300$ K, $p_{O_2} \sim 10^{-4}$ bar). However, we note that the estimate of δ for the thicker films may be to large, so that the resulting value of Γ is too low and the value of the O chemical potential $\Delta\mu_{\rm O} \geq -2$ eV is too high. In any case, at not too high temperatures, and not too low pressures the $Al_{4n-4}O_{6n}$ stoichiometries will always be stabilized.
[37] F. C. Chuang *et al.*, Surf. Sci. **573**, L375 (2004).
[38] M. Sierka *et al.*, J. Chem. Phys. **126**, 234710 (2007).
[39] J. Rohrer and P. Hyldgaard, unpublished.
[40] This statement is based on geometrical grounds (large separations between TiC/O and the alumina). A more quantitative discussion of the anchoring of thin $Al_{4(n-1)}O_{6(n-1)}$ films on TiC/O and $Al_{4n-2}O_{6n}$ films on TiC will be given elsewhere.
[41] J. Rohrer, C. Ruberto, and P. Hyldgaard, unpublished.